Nanoindentation of the *a* and *c* domains in a tetragonal $BaTiO_3$ single crystal

Young-Bae Park and Matthew J. Dicken
Thomas J. Watson Laboratory of Applied Physics, California Institute of Technology, Pasadena, California 91125, USA

Zhi-Hui Xu[a] and Xiaodong Li[b]
Department of Mechanical Engineering, University of South Carolina, 300 Main Street, Columbia, South Carolina 29208, USA

(Received 1 July 2007; accepted 17 August 2007; published online 17 October 2007)

Nanoindentation in conjunction with piezoresponse force microscopy was used to study domain switching and to measure the mechanical properties of individual ferroelectric domains in a tetragonal $BaTiO_3$ single crystal. It was found that nanoindentation has induced local domain switching; the *a* and *c* domains of $BaTiO_3$ have different elastic moduli but similar hardness. Nanoindentation modulus mapping on the *a* and *c* domains further confirmed such difference in elasticity. Finite element modeling was used to simulate the von Mises stress and plastic strain profiles of the indentations on both *a* and *c* domains, which introduces a much higher stress level than the critical value for domain nucleation. © *2007 American Institute of Physics*.
[DOI: 10.1063/1.2795664]

I. INTRODUCTION

Bulk crystals and thin films of various ferroelectric materials such as $BaTiO_3$ are of interest because of their superior dielectric, pyroelectric, piezoelectric, and electro-optic properties for numerous potential applications in microelectronic devices, sensors, and micro/nanoelectromechanical systems (MEMS/NEMS). It is well known that the application of mechanical stress or electrical field can change the domain structure in ferroelectrics.[1–6] The mechanical properties of constitutive domains may influence the functionality and the reliability of the ferroelectric devices. Moreover, as the size of a ferroelectric device shrinks down to micro/nanolevel, its components consist of only a few domains and the mechanical properties of individual domains play a critical role in the design, fabrication, and function of the whole device. Surprisingly, the mechanical properties of individual domains in ferroelectrics are still lacking. This raises the first issue: are the mechanical properties of the *a* and *c* domains the same in ferroelectrics? If not, what is the difference in Young's modulus and strength between the *a* and *c* domains? On the other hand, in the manufacturing processes and practical applications of micro/nanodevices, mechanical impact loading often occurs at the component surfaces/interfaces.[7,8] For instance, the actuating properties in the ferroelectric MEMS/NEMS are fundamentally based on the mechanical stress/strain behavior of ferroelectric materials. Such mechanical stress may cause domain switching and/or phase transition (symmetry change),[5,10] thereby inducing local stress and strain and then leading to malfunction or failure of the whole device. This raises the second issue: can nanoscale impact loading induce domain structure change? Thus, a fundamental understanding of domain nanomechanics and nanoresponse under nanomechanical loading is needed for the future success of these novel applications.

The extremely small dimensions of constitutive ferroelectric domains impose great challenges to many existing testing and measuring techniques for experimental studies of their mechanical properties. The atomic force microscopy (AFM) with piezoresponse mode, also called piezoresponse force microscopy (PFM), has been paid much attention in domain imaging since it was developed in 1991.[9–11] The surface morphology and *in situ* piezoresponse signal image can be obtained by PFM. The nanoindenter is maturing as an important tool for probing the mechanical properties of small volumes of material.[12–14] The recently developed nanoindenter has the capability of measuring surface morphology at nanoscale by scanning the sample surface with the same indenter tip, which is analogous to AFM contact mode.[15] Such nanoindenter/AFM combination provides the "eyes" and "tools" for imaging and testing individual ferroelectric domains at nanoscale. Postnanoindentation PFM imaging provides the capability of verifying if the indentation test was performed in the anticipated domain as well as detecting domain switching in nanoindentation.

In this study, using nanoindentation and PFM, we report, for the first time, results of mechanical properties of individual *a* and *c* domains, including their deformation behavior such as strain and stress distributions in the indented region. Here we show that the emerging technique of scanning nanoindentation can be used to obtain modulus mapping across the *a* and *c* domains, revealing significant differences in elastic modulus between these domains. We also discovered that nanoindentation induced domain switching. These results are critical for accurate nanomechanical modeling of domain behavior in ferroelectrics as well as for design, manufacturing, and application of ferroelectric materials.

[a]Electronic mail: xuzhihui@engr.sc.edu
[b]Author to whom correspondence should be addressed. Electronic mail: lixiao@engr.sc.edu

II. EXPERIMENTAL DETAILS

A bulk tetragonal $BaTiO_3$ single crystal with Curie temperature of 125 °C was grown by Bridgman method [double side polished, (001) orientation, $10\times10\times1$ mm^3 from MTI or GmMatech, Germany]. Polarized optical microscopy (POM) and contact mode atomic force microscopy (Autoprobe CP-R, Veeco Metrology Group) were used to image and assign individual domains. In the AFM imaging, topographic and PFM modes were used to obtain both surface morphology and domain structural information *in situ*. The PFM imaging allows the measurement of the local converse piezoelectric displacement of individual ferroelectric domains. The piezoelectric response signal (PRS) from tip deflection (out-of-plane polarization vector component) was obtained by lock-in amplifier techniques. The PFM imaging was performed using highly doped *n*-type-silicon cantilevers of triangular geometry, which were modulated with an ac voltage of 3–5 V, resonance frequency of 1–2 kHz, and scan rate of 0.3 Hz. X-ray diffraction (XRD) (Rigaku, D/MAX-RC) and reflected high electron energy diffraction (RHEED) analysis techniques were used to identify phase structure and crystalline orientation.

Nanoindentation tests were performed using a Triboscope nanomechanical testing system (Hysitron Inc.) in conjunction with a Veeco Dimension 3100 AFM system (Veeco Metrology Group). The nanoindenter monitored and recorded the load and displacement of the Berkovich indenter, a diamond three-sided pyramid, with a force resolution of about 1 nN and a displacement resolution of about 0.1 nm. A typical indentation experiment consisted of three subsequent steps: approaching the surface, loading to peak load, and finally unloading completely. A series of nanoindentations were made on individual *a* and *c* domains of the $BaTiO_3$ with a peak indentation load of 5 mN. The hardness and elastic modulus were calculated from the nanoindentation load-displacement curves using the Oliver and Pharr method.[12]

Combining with a SR830 DSP dual phase lock-in amplifier (Stanford Research Systems), the nanoindentation system can also be used for dynamic testing of materials, e.g., modulus mapping test, by scanning and simultaneously indenting the $BaTiO_3$ surface. A cube corner diamond tip with a nominal tip radius about 50 nm was used for the modulus mapping. During modulus mapping, the electrostatic force acting on the spring-suspended center plate of the force-displacement transducer was sinusoidally modulated at 200 Hz, while the tip attached to the transducer was scanning the sample surface. The amplitude and the phase of the resulting transducer displacement signals were measured with the lock-in amplifier and used to determine the local indentation moduli of the sample at each pixel of a 256×256 pixel image. Typically, a displacement amplitude of 1 nm was used for modulus mapping with a dynamic force of about 1 μN. Three different images, named contact force, contact stiffness, and elastic modulus, were simultaneously acquired during the modulus mapping.

III. RESULTS AND DISCUSSION

The surface and domain structures of ferroelectric materials have been well established and reported. Figure 1(a) shows a typical schematic of ferroelectric domains with the tetragonal structure. The bottom two lines in Fig. 1(a) represent typical PRS intensity along the alternative *a-c* domains from PFM measurement and a corresponding topographical height profile from AFM measurement, respectively.[16] The tetragonal angle of the $BaTiO_3$, which is in a point group *Cv* 4*mm*, is typically 0.4°–0.6° below Curie temperature which can be obtained by $d\theta=2\arctan(c/a)-90°$, where *a* and *c* are lattice parameters (c/a ratio=1.016). Positive domains (c^+ domains), polarization downward, show a higher PRS, while *a* domains show a lower PRS which shows zero PRS in the out-of-plane PFM measurement. The schematic feature of ferroelectric domains includes 90° domain walls found in the $BaTiO_3$. The arrows in the figure indicate [001] and [100] orientations of polarization.

Figure 1(b) shows the POM image of the $BaTiO_3$. The domain size was measured to be in the range from 2 to 10 μm. The *c* and *a* domains represent dark and white colors in the POM image, respectively. The black and white stripes are due to the bifringence effect of ferroelectric domains. Many domains are overlapped in the transmittance-mode OM image through 1 mm thick $BaTiO_3$ crystal. During the crystal preparation such as polishing and annealing, fine single crystal domains are formed in order to reduce strain energy with a thermodynamically stable tetragonal $BaTiO_3$ at room temperature.

Figure 1(c) shows reciprocal phase measurements of the $BaTiO_3$ using XRD and RHEED techniques. The XRD spectrum shows typical (001)/(100) peak splitting due to the *a-c* domain overlapping through the probing thickness and beam spot size of the x-ray diffractometer. Holt *et al.* and Rogan *et al.* reported microfocused x-ray experiment using Fresnel zone plate optics which allows 0.3 μm spartial resolution.[2,3] They showed asymmetric strain profile along the $a/c/a/c$ domain strips. However, still domain wall region could not be resolved well because of the limitation of x-ray beam size regarding the ferroelectric domain wall thickness and smaller scale domain structures.

Anisotropic nature of ferroelectric domain property is often due to stress and dielectric permittivity. Wang *et al.* measured dielectric constant and loss tangent along the $a/c/a/c$ domain structure using near-field scanning microwave microscopy.[17] They observed that the origin of anisotropy came from the anisotropy of the dielectric constant and the tilt of *a-c* domain walls with respect to the surface normal, as shown in Fig. 1(a). While our AFM and PFM results also showed similar anisotropic nature of piezoresponse signal along the *a-c* domain walls, in this study, we mostly focused on the nanomechanical properties of the a/c domains and will discuss more detail of the anisotropic nature along the a/c domains regarding strain profile and electrodynamics elsewhere.

Prior to nanoindentation test, we investigated the $BaTiO_3$ crystal and located the positions of interest to be indented. The AFM and PFM images of the $BaTiO_3$ obtained

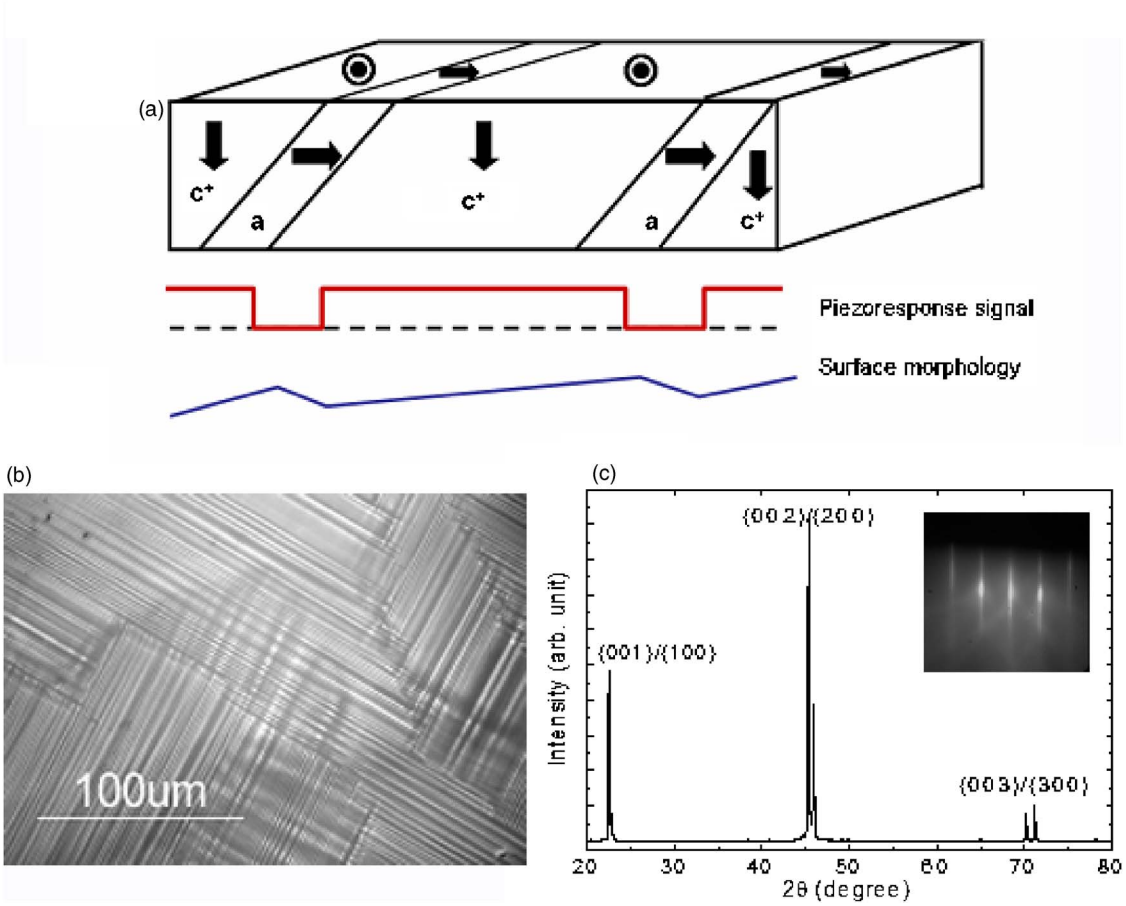

FIG. 1. (Color online) (a) Schematic feature of ferroelectric domains including 90° domain walls found in ferroelectric $BaTiO_3$. The arrows indicate [001] and [100] orientations of polarization. Bottom lines represent piezoreponse signal intensity from PFM and topographical height profile from AFM, respectively. (b) XRD and RHEED patterns for crystal orientation and surface crystal structure. (c) POM image shows typical 90° domain wall.

simultaneously using contact AFM are shown in Figs. 2(a) and 2(b). The AFM image of the $BaTiO_3$ surface shows the typical tetragonal corrugation features as described in Fig. 1, which are the typical surface corrugation feature and the typical butterfly pattern domain arrangement. The domain size measured from the AFM is in good agreement with the result obtained from POM and the surface corrugation angle ($\Delta\theta$) is 0.5°–0.6° which confirms tetragonal 90° $BaTiO_3$ domain wall. In the piezoresponse image, the bright and dark areas originate from the downward (c^+) and lateral polarized (a) domains, respectively.

In conjunction with the AFM and PFM observations, it can be clearly seen that the $BaTiO_3$ contains a lamellar shape 90° domain structure composed of alternating c^+ and a^+ (or a^-) domains. The black line profile, as seen in Fig. 2(c), shows the PRS intensity along the $a/c/a/c$ multidomains before the nanoindentation. After confirming the domain characteristics using the AFM and PFM, nanoindentations were performed on individual a and c domains to study their nanomechanical properties and deformation behavior. After the nanoindentations, the AFM and PFM were performed in the same area to detect the indentation-induced domain switching, as seen in Figs. 2(a) and 2(b).

With the nanoindentation, the c^+ domain switched to c^- (180° domain switching) and a domain switched to c^- (90° domain switching) regarding line profiles of the PR signal in Fig. 2(c). Mechanical stresses introduced by nanoindentation cause the 180° and 90° domain switching. Red color line in the middle of the indented region, as indicated by the arrow in Fig. 2(c), is due to 180° domain switched c^- component of polarization. On the other hand, the pileup region around the indented region shows gray color and it means a plastic deformation or 90° domain switching. These domain-switching phenomenon requires further PFM (in-plane piezoresponse) and crystallographic studies in future work. The nanoindentation-induced domain-switching mechanism can be used to modify the local nanoscale domain structures to realize multifunctional micro/nanodevices. In addition, mechanical impact loading can in turn generate local electrical field at the nanoscale to store energy and/or to modify local polarity of domain.

Figure 3 shows the representative load-displacement curves of nanoindentations made on a and c domains together with the corresponding finite element modeling (FEM) simulation results, respectively. The tested a and c domains of $BaTiO_3$ have a domain width about 2–10 μm. These a and c domains form a mixed stacking multilayer structure with a layer thickness about 100–500 μm. The maximum penetration depth of nanoindentation on individual domain was kept less than 150 nm in this study, which precludes the possible effect on the mechanical properties measured by nanoindentation from the neighbor do-

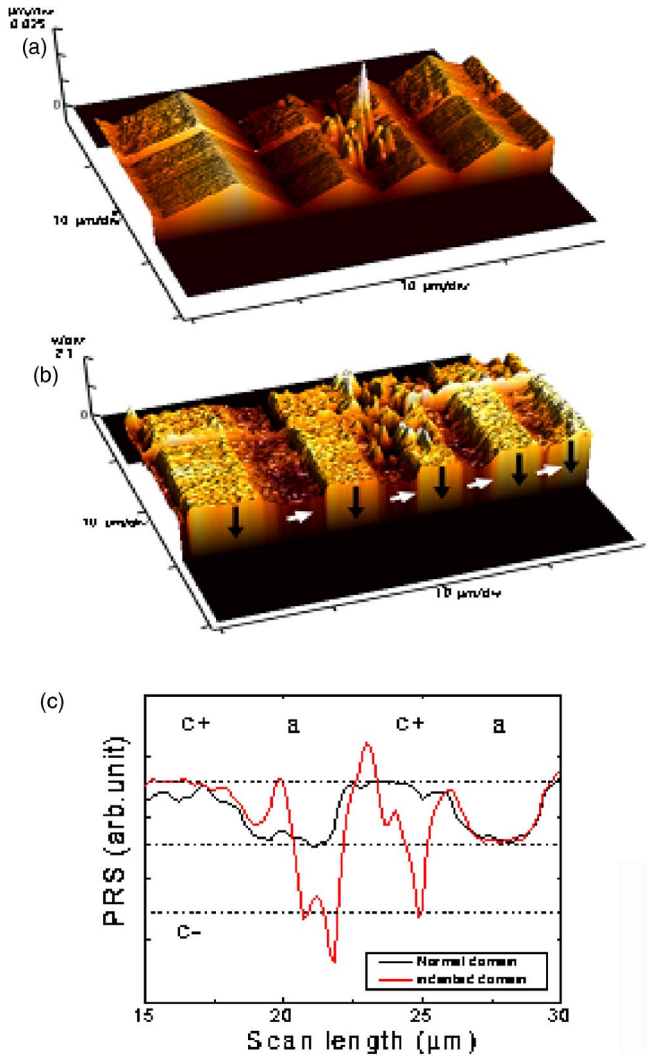

FIG. 2. (Color online) (a) Real space AFM imaging of ferroelectric $BaTiO_3$ in room temperature where $BaTiO_3$ shows typical tetragonal corrugation feature. AFM image of single crystal $BaTiO_3$ surface was performed in 40 $\times 40$ μm^2 scan, (b) PFM image, and (c) line scanning of PRS along the *c*-*a* domains.

mains and the underneath layer.[18,19] As shown in Fig. 3, the load-displacement curves of *a* and *c* domains are different from each other, indicating that *a* and *c* domains have different mechanical properties. Under the same peak indentation load, the displacement of *a* domain is apparently less than that of *c* domain. This suggests that *a* domain is harder and stiffer than *c* domain. Using the same Poisson's ratio of 0.3 for both *a* and *c* domains, the elastic modulus of *a* domain was calculated to be 154.16±1.92 GPa from the load-displacement curves, which is higher than that of *c* domain with a value of 139.59±2.55 GPa. The elastic moduli of *a* and *c* as well as the *c*/*a* ratio are consistent with Refs. 20 and 21. The hardnesses of *a* and *c* domains are comparable, which are 13.94±0.26 GPa for *a* domain and 13.02±0.5 GPa for *c* domain. Nanoindentations with a sharper cube corner indenter also showed that there is no hardness difference between *a* and *c* domains[20] though the hardness values measured with the cube corner are a bit larger than the values measured with blunt Berkovich indenter in this study.

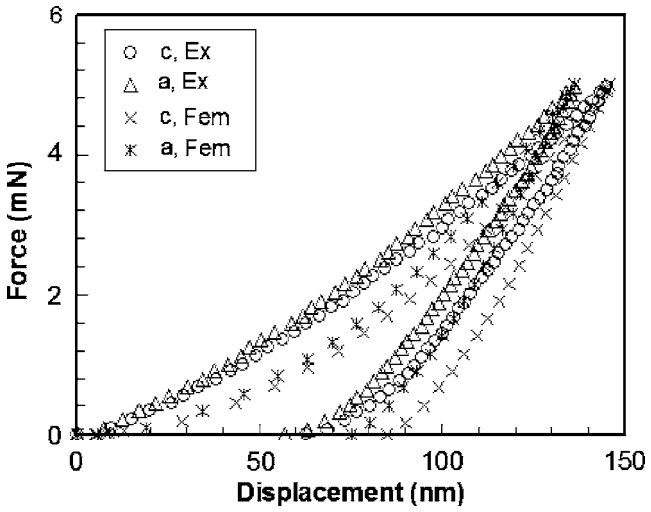

FIG. 3. Experimental and finite element simulation force-displacement curves of nanoindentations on *a* and *c* domains of $BaTiO_3$. The elastic modulus and hardness measured by nanoindentation test are 135.28±2.55 and 13.02±0.5 GPa for *c* domain and 147.58±1.92 and 13.94±0.26 GPa for *a* domain.

To further study the difference in elastic modulus between *a* and *c* domains, nanoindentation modulus mapping experiments were performed along the *a*/*c*/*a*/*c* domains. Contact force, contact stiffness, and elastic modulus were simultaneously acquired when the nanoindenter tip scanned and indented the sample surface. The results of the modulus mapping of *a* and *c* domains of $BaTiO_3$ are shown in Fig. 4. Figure 4(a) shows the three dimensional (3D) topography of *a* and *c* domains where the modulus mapping was performed. The contact forces on both domains are uniform in the modulus mapping area [Fig. 4(b)], while the contact stiffness [Fig. 4(c)] and modulus [Fig. 4(d)] show a sharp difference between *a* and *c* domains. Clearly *a* domain has a higher modulus than *c* domain, as shown in Fig. 4(e).

As expected, the modulus mapping results show the same trend as the nanoindentation test. However, the data of modulus mapping have a larger scatter compared with nanoindentation test. This may be due to the surface roughness which definitely has a bigger effect on the accurate determination of contact area at shallow penetration (1 nm) for modulus mapping than at deep penetration (about 140 nm) for nanoindentation.

To evaluate the stress and strain fields produced by nanoindentation, 3D FEM simulation was performed to simulate the nanoindentations made on *a* and *c* domains with Berkovich indenter. The elastic moduli of *a* and *c* domains measured by nanoindentation as shown above were used as an input for the FEM simulation. The yield stresses of *a* and *c* domains are estimated from the nanoindentation hardnesses using the following equations:[22]

$$\ln\left(\frac{H}{E}\right) = 0.8503 \ln\left(\frac{\sigma_y}{E}\right) + 0.2456. \quad (1)$$

A linear strain hardening behavior was adopted for the simulation so that the load-displacement curve from FEM simulation predicts the same penetration depth at same peak indentation load as the experiment, as shown in Fig. 3. The

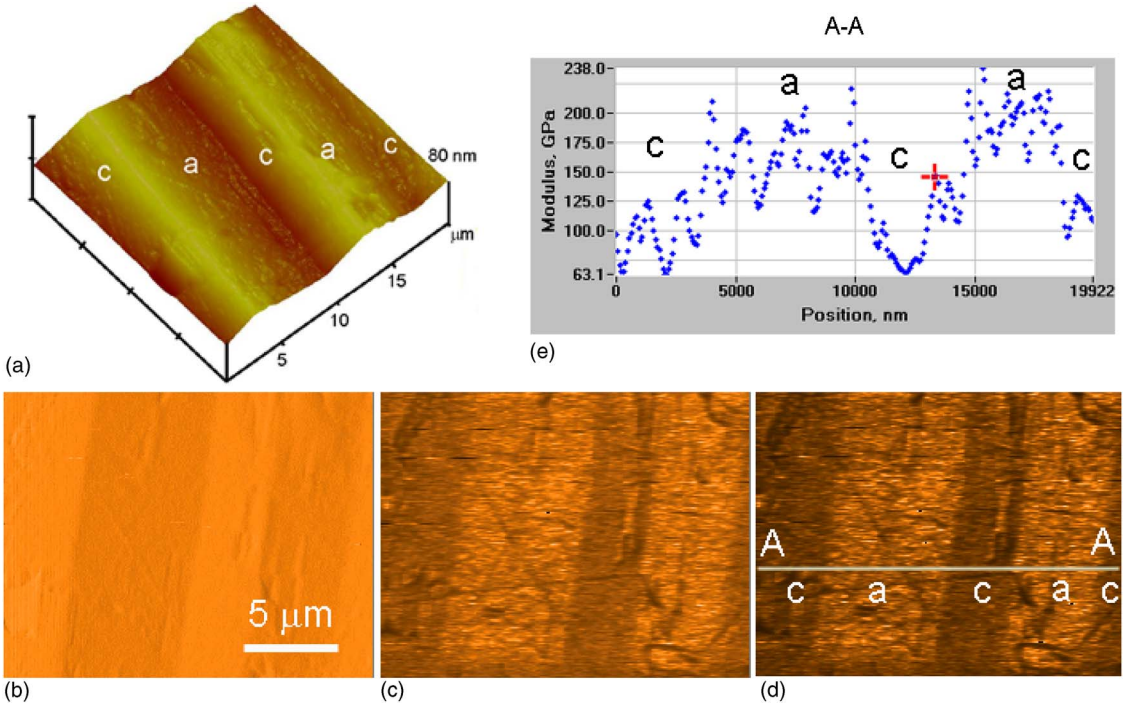

FIG. 4. (Color online) Elastic modulus mapping of $BaTiO_3$ showing modulus difference in *a* and *c* domains. (a) 3D topography of *a* and *c* domains, (b) contact force image, (c) contact stiffness image, (d) modulus image, and (e) modulus variation along line A-A.

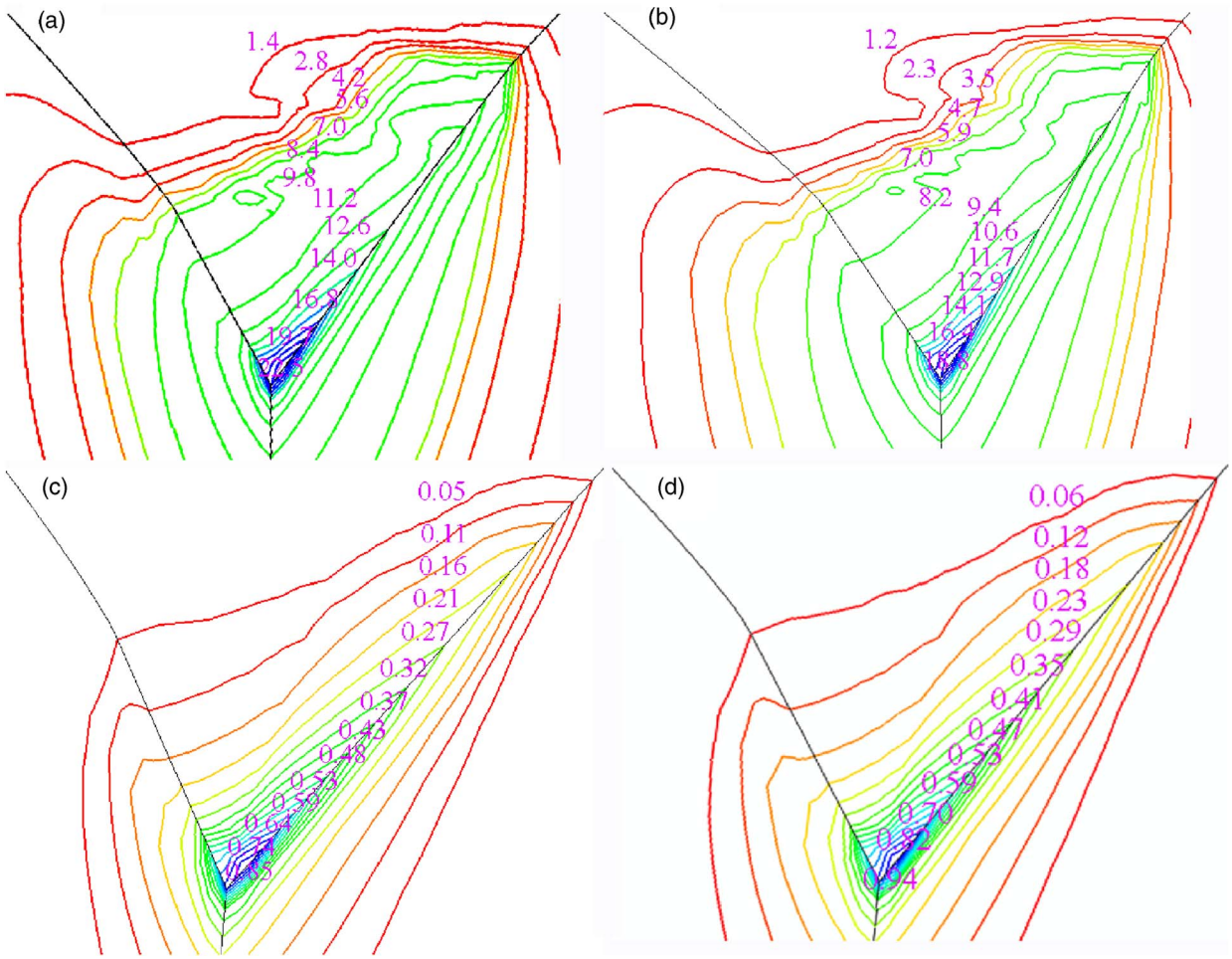

FIG. 5. (Color online) von Mises stress [(a) and (b)] (in GPa) and equivalent plastic strain [(c) and (d)] fields of nanoindentation on each $BaTiO_3$ domain with a Berkovich indenter. (a) and (c) for *a* domain; (b) and (d) for *c* domain using FEM simulation.

stress and strain fields induced by nanoindentation on *a* and *c* domains are shown in Fig. 5. As can be seen, the von Mises stress [Fig. 5(a)] of *a* domain is larger than that of *c* domain [Fig. 5(b)], whereas the equivalent plastic strain [Fig. 5(c)] created in *a* domain is smaller than that of *c* domain [Fig. 5(d)]. Apparently the stress field created by nanoindentation is much higher than the critical value for domain nucleation (0.22 MPa) or removal (1.1 MPa).[6] The existence of the high stress and strain field in the $BaTiO_3$ under nanoindentation leads to ferroelectric domain switching, which in turn influences the force-displacement curve of nanoindentation. Although we observed local domain switching for individual indented spots, the spatial domain switching in local indented region will be discussed elsewhere.

IV. CONCLUSION

The mechanical properties of individual *a* and *c* domains were measured by nanoindentation in conjunction with piezoresponse force microscope (PFM). The *a* and *c* domains show comparable hardness but a significant difference in elastic modulus. The elastic modulus mapping across the *a* and *c* domains also revealed such a difference between the *a* and *c* domains. Nanoindentation-induced domain switching was discovered. The stress and strain distributions in the indented regions in the *a* and *c* domains obtained by FEM simulation indicate a much higher stress level than the critical value for domain nucleations.

ACKNOWLEDGMENTS

This work has been supported by the National Science Foundation (Grant No. EPS-0296165) and the University of South Carolina NanoCenter.

[1] J. Y. Li, R. C. Rogan, E. Ustundag, and K. Bhattacharya, Nat. Mater. **4**, 776 (2005).
[2] R. C. Rogan, N. Tamura, G. A. Swift, and E. Ustundag, Nat. Mater. **2**, 379 (2003).
[3] M. Holt, Kh. Hassani, and M. Sutton, Phys. Rev. Lett. **95**, 085504 (2005).
[4] Y. B. Park, J. L. Ruglovsky, and H. A. Atwater, Appl. Phys. Lett. **85**, 455 (2004).
[5] F. Fang and W. Yang, Mater. Lett. **57**, 198 (2002).
[6] Z. Li, C. M. Foster, X. H. Dai, S. K. Chan, and D. J. Lam, J. Appl. Phys. **71**, 4481 (1992).
[7] X. D. Li, B. Bhushan, K. Takashima, C.-W. Baek, and Y.-K. Kim, Ultramicroscopy **97**, 481 (2003).
[8] X. D. Li and B. Bhushan, Surf. Coat. Technol. **163–164**, 503 (2003).
[9] P. Gunther and K. Dransfeld, Appl. Phys. Lett. **61**, 1137 (1992).
[10] J. Munoz-Saldana, G. A. Schneider, and L. M. Eng, Surf. Sci. **480**, L402 (2001).
[11] D. Shilo, G. Ravichandran, and K. Bhattacharya, Nat. Mater. **3**, 453 (2005).
[12] W. C. Oliver and G. M. Pharr, J. Mater. Res. **7**, 1564 (1992).
[13] B. Bhushan and X. D. Li, Int. Mater. Rev. **48**, 125 (2003).
[14] X. D. Li and B. Bhushan, Mater. Charact. **48**, 11 (2002).
[15] X. D. Li, H. S. Gao, C. J. Murphy, and K. K. Caswell, Nano Lett. **3**, 1495 (2003).
[16] S. V. Kalinin, C. Y. Johnson, and D. A. Bonnell, J. Appl. Phys. **91**, 3816 (2002).
[17] Y. G. Wang, M. E. Reeves, and F. J. Rachford, Appl. Phys. Lett. **76**, 3295 (2000).
[18] Z. H. Xu and D. Rowcliffe, Thin Solid Films **447**, 399 (2004).
[19] Z. H. Xu and X. D. Li, Acta Mater. **54**, 1699 (2006).
[20] T. Scholz, J. Munoz-Saldana, M. V. Swain, and G. A. Schneider, Appl. Phys. Lett. **88**, 091908 (2006).
[21] R. Bechmann, R. F. S. Hearmon, and S. K. Kurtz, *Numerical Data and Functional Relationships in Science and Technology*, Landolt-Bornstein, New Series, Group III (Springer, Berlin, 1969), Vol. 2.
[22] Z. H. Xu and D. Rowcliffe, Philos. Mag. A **82**, 1893 (2002).